ACS OMEGA

http://pubs.acs.org/journal/acsodf

Article

Effect of Structural Parameters on the Performance of Axial-Flow Inlet Hydrocyclones for In Situ Desanding from Natural Gas Hydrate Mixed Slurry

Shunzuo Qiu,* Lin Zhong, Guorong Wang, Xing Fang, Yan Yang, and Qin Liu

Cite This: *ACS Omega* 2023, 8, 28531−28542

Read Online

ACCESS | Metrics & More | Article Recommendations

ABSTRACT: Structural parameters play a decisive role in the performance of hydrocyclones for in situ natural gas hydrate (NGH) recovery and desanding. In this paper, the effects of key structural parameters on its performance were investigated by numerical simulations and experimental methods. The results show that the most influential factors are the spiral pitch of the spiral inlet, the vortex finder diameter, and the spigot diameter. The second most influential factors are the spiral turn number and the cone angle. Other parameters have the least influence. Specifically, the NGH recovery efficiency and pressure drop increase, but desanding efficiency decreases as d_0/D and the cone angle increase. The NGH recovery efficiency and pressure drop decrease and desanding efficiency increases as d_s/D increases. Therefore, it is necessary to choose a suitable value to balance the efficiency and pressure drop to improve the performance, for example, selecting the appropriate diameter ratio of the vortex finder and spigot. The above results can be used for the engineering design of in situ separators in marine hydrate mining and further realize in situ desanding, NGH recovery, and sand backfilling.

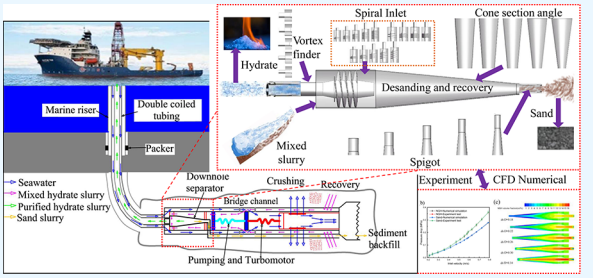

1. INTRODUCTION

Natural gas hydrate (NGH) is an ice-like solid substance formed by the combination of methane or other gases with water under high pressure and low temperature.[1,2] Exploration practice has proved that the NGH resource is a huge and potential substitute resource in the future.[3] Marine shallow NGHs are widely distributed all over the world, and their reserves are huge. They have been established as the 173rd mineral type in China medium and long-term scientific and technological development plan. In 2017, marine gas hydrate trial production was implemented successfully in the South China Sea.[4,5] In 2020, the second trial production of the South China Sea produced a total gas of 861,400 m^3 and an average daily gas production of 28,700 m^3,[6,7] realizing a phased leap from "exploratory trial production" to "experimental trial production," a step closer to commercial development. However, NGH test production in existing sea areas is mostly limited by sand production.[8] In particular, China's marine hydrates are mostly found in unconsolidated, weakly consolidated, or fractured argillaceous silt reservoirs with frequent "three shallow" disasters,[9,10] which is the limitation of conventional oil and gas sand control technology. And the phenomenon of sand production is unavoidable in the process of NGH exploitation, which is one of the bottleneck problems that hinders its development for long-term commercial use.

To solve the problem of sand production, traditional sand control tools such as GeoFORM composites, sand control screens, casing-surrounding gravel, and other pipe-type mechanical sand control tools were used in the trial mining in Japan and China in 2017 and 2020.[11−13] The above technologies for NGH sand control all have certain shortcomings, such as high-precision sand control, leading to increased resistance, serious reduction of the fluid flow rate, and blockage of the wellbore and reservoir, resulting in reduced productivity. The principle of solid fluidization development of deep-water shallow hydrate reservoirs was proposed by the academician Zhou.[5] One of the key components of the method is to remove sand from the broken NGH-mixed slurry in situ and put the sand back on the seafloor. The principle of mining and sand removal is shown in Figure 1.[14] The new method can prevent wellbore and reservoir blockage while maintaining productivity and even effectively reduce the risk of subsea reservoir collapse.

Hydrocyclones were widely used in the fields of the petroleum industry,[15−18] chemical industry,[19] mineral processing,[20,21] environmental protection, and biology due to their simple design, high separation efficiency, large processing

Received: April 28, 2023
Accepted: July 11, 2023
Published: July 27, 2023

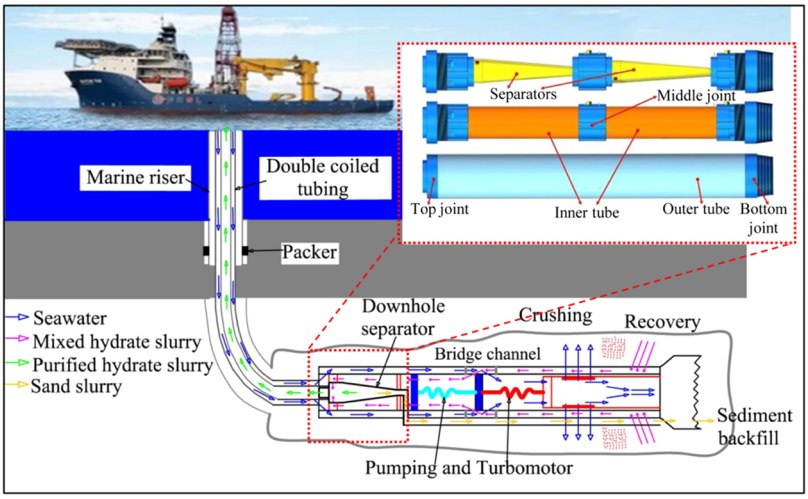

Figure 1. Technology and process of exploitation of NGH.[14]

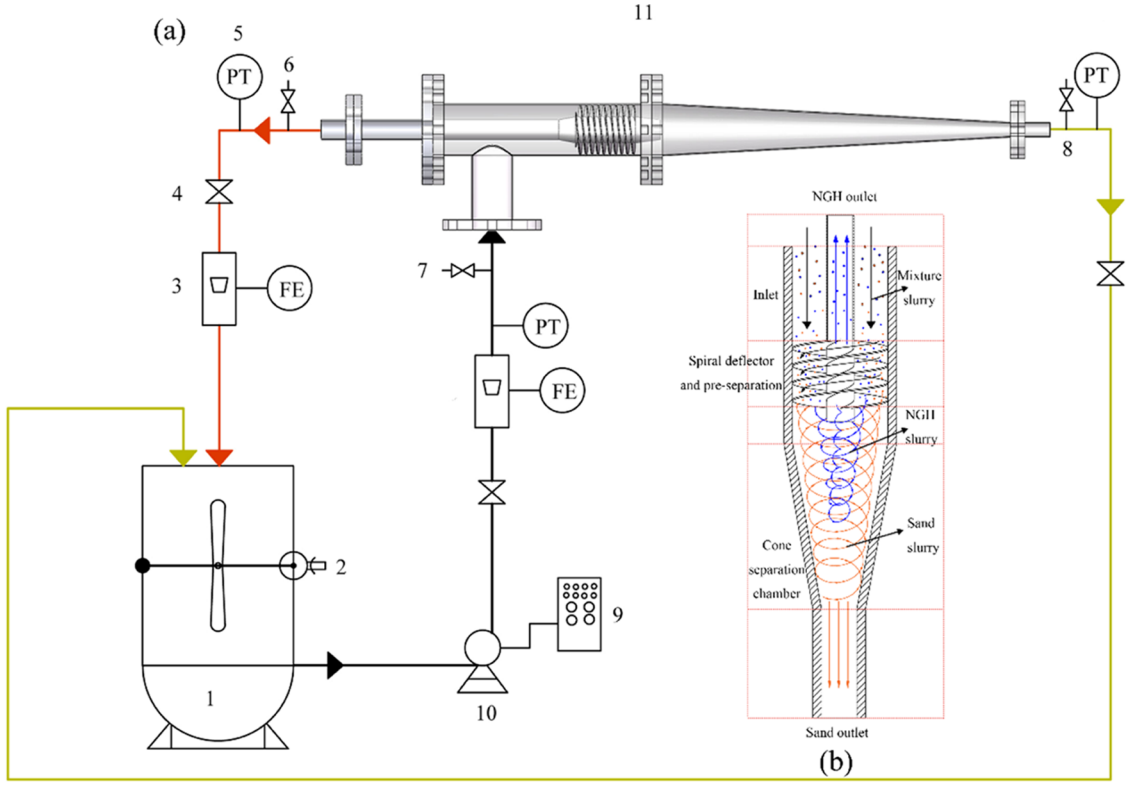

Figure 2. (a) Experimental equipment for NGH separation and (b) the principle of separation of the NGH hydrocyclone.

capacity, and low operation and maintenance costs. For the hydrocyclone used for in situ desanding to purify NGH, certain research, mainly from the aspects of the internal flow field, separation performance, and structural design, has been carried out. Wang[22,23] et al. proposed a new type of hydrocyclone, taking pure mortar as the research object, without considering hydrate particles in the slurry, revealing the relationship between pipeline flow, structural parameters, and sand particle movement speed, trajectory, etc., and established a computational fluid dynamics (CFD) numerical calculation model to obtain the relationship between the flow rate and separation efficiency under a specific structure. Wu[24,25] et al. analyzed the force and motion trajectory of the particles in the spiral tube and revealed the particle separation mechanism. Wang[26−29] et al. combined the test mining parameters and considered the effect of phase transition, and used the numerical simulation method to reveal the particle motion trajectory, phase distribution, and separation efficiency in the classical tangential inlet hydrocyclone and spiral separator. The effect of spiral inlet geometric parameters on the performance of the NGH axial-flow inlet hydrocyclone was investigated, and the influence laws were obtained among the published articles by the author.[14] However, all structural parameter configuration plays a decisive role in the performance of specific NGH hydrocyclones.

Therefore, the purpose of this paper is to reveal the influence of structural parameters on separation performance. In detail, the sensitivity of the influence of structural

https://doi.org/10.1021/acsomega.3c02920
ACS Omega 2023, 8, 28531−28542

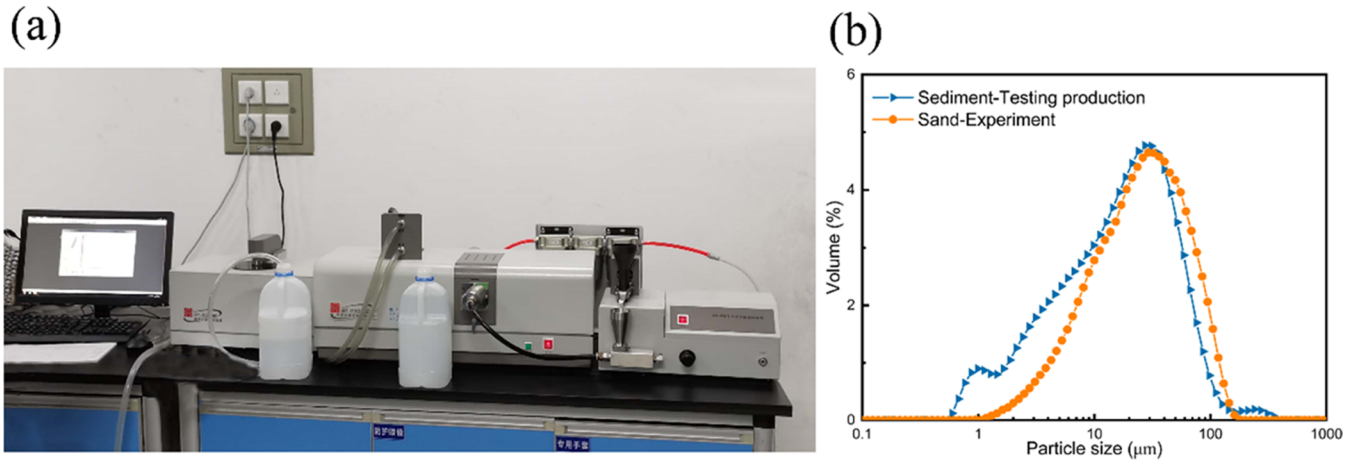

Figure 3. (a) BT-9300LD dry and wet laser particle size analyzer and (b) size distribution of the material.

parameters on separation efficiency and pressure drop was investigated, and the single sand removal experiment was carried out for model validation. Then, the effects of the d_0/D, d_s/D, and cone angle on tangential velocity, pressure, discrete phase distribution, separation efficiency, and pressure drop were observed using the numerical simulation because separation efficiency and pressure drop are the most important indicators for evaluating the performance of a hydrocyclone. In order to explain the inherent mechanism of the relationship between separation efficiency, pressure drop, and structural parameters, it is necessary to reveal the distribution law of discrete phases, the relationship between tangential velocity and pressure to structural parameters.

2. EXPERIMENT AND NUMERICAL SIMULATIONS

2.1. Experimental Methods. *2.1.1. Experimental Materials and Setup.* The separation experiment is shown in Figure 2. The amount of sand added to the mixing tank was calculated according to the proportion of the solid volume concentration. As presented in Figure 3b, the particle size was prepared according to the particle size distribution obtained from the South China Sea trial mining. The sand particles with the required particle size are selected with a standard screen and then a BT-9300LD dry and wet laser particle size analyzer shown in Figure 3a. In the single-phase sand separation experiment, the amount of sand added to the mixing tank was calculated according to the proportion of 15 vol %. The quartz sand was selected. The physical parameters of the media in the experiment are shown in Table 1.

Table 1. Physical Parameters of Media in the Experiment

media	density (kg/m^3)	viscosity (kg/m/s)
water	1000	
quartz sand	2650	

2.1.2. Analytical Method. The gravimetric method was used to determine inlet and outlet solids content. First, the volume of the collected suspension sample was measured and recorded. The suspension samples were then vacuum filtered. The solid particles obtained after suction filtration were dried at a constant temperature and weighed. The solid content can be expressed as

$$C = \frac{m}{V} \tag{1}$$

where C is the solid content (g/L), m is the mass of the particles after suction filtration and drying at constant temperature (g), and V is the total volume of the collected suspension sample (L).

Thus, the separation efficiency formula is

$$E_2 = \frac{C_2 \times Q_2}{C \times Q} \tag{2}$$

where E_2 is the desanding efficiency (%), C_2 is the solid content at the sand slurry outlet (g/L), Q_2 is the flow at the sand slurry outlet (L/h), C is the solid content at the inlet (g/L), and Q is the inlet flow (L/h).

2.2. Numerical Simulations. *2.2.1. Numerical Model. 2.2.1.1. Mixture Model.* In the numerical simulation, the correct choice of the multiphase flow model is very important for the accurate description of the characteristics of the multiphase flow basin. Common multiphase flow models mainly include the volume of fluid (VOF), mixed, and Euler−Euler models. The volume of fluid (VOF) multiphase model was used to predict the air core of the water−air system. While the Euler−Euler model is basically the correct model, it is much more complicated. The mixed model is a simplification of the Euler−Euler model, which has the characteristics of calculation accuracy and speed and is mainly used for thick pulp. And in this paper, the solid concentration is 25%. It is a high solid concentration. Therefore, the mixed multiphase flow model is adopted.

The continuity equation is as follows:[30]

$$\frac{\partial \rho}{\partial t} + \frac{\partial \rho u_i}{\partial x_i} = 0 \tag{3}$$

The momentum equation of the mixture model is as follows:[30]

https://doi.org/10.1021/acsomega.3c02920
ACS Omega 2023, 8, 28531−28542

$$\frac{\partial}{\partial t}(\rho u_i) + \frac{\partial}{\partial x_j}(\rho u_i u_j) = -\frac{\partial}{\partial x_i}p + \frac{\partial}{\partial x_i}\left(\sum_{k=3}^{n} p_k\right) + \frac{\partial}{\partial x_j}\left[\mu\left(\frac{\partial u_i}{\partial x_j} + \frac{\partial u_j}{\partial x_i}\right) + (-\rho\overline{u_i' u_j'}) + \sum_{k=1}^{n} \rho_k u_{\mathrm{dr},ki} u_{\mathrm{dr},kj}\right] + g\rho \quad (4)$$

where u_{dr} is the drift velocity, g is the gravitational acceleration, $-\rho\overline{u_i' u_j'}$ is the Reynolds stress term, and u_j, u_i, and ρ are the velocities and density of the mixture phase fluid, respectively, which are defined as equations[30]

$$\rho = \sum_{k=1}^{n} \alpha_k \rho_k,\ u_i = \frac{\sum_{k=1}^{n} \alpha_k \rho_k u_{k,i}}{\rho},\ \mu = \sum_{k=1}^{n} \alpha_k \mu_k \quad (5)$$

where μ_k, α_k, ρ_k, and u_k are the viscosity, volume fraction, density, and velocity of the kth phase fluid, respectively.

2.2.1.2. RSM Model. Considering that the swirling field is a strong turbulent flow field, the choice of the turbulence model plays a key role in accurately simulating the turbulent behavior of the flow field in the cyclone. The Reynolds stress model (RSM) has proven to be an accurate simulation of hydrocyclones because it takes into account the effects of rapid changes in water curvature, rotation, eddy currents, and strain. Therefore, this study chooses RSM for simulation research.

The RSM model transport equation can be written as[30,31]

$$\frac{\partial(\rho\overline{u_i' u_j'})}{\partial t} + \frac{\partial(\rho u_k \overline{u_i' u_j'})}{\partial x_k} = D_{T,ij} + D_{L,ij} + P_{ij} + \phi_{ij} + \varepsilon_{ij} + F_{ij} \quad (6)$$

where $D_{L,ij}$ is the molecular diffusion, $D_{T,ij}$ is the turbulent diffusion, ϕ_{ij} is the pressure strain, ε_{ij} is the dissipation, F_{ij} is the production by system rotation, and P_{ij} is the stress production.

2.2.2. Boundary Conditions. The whole process of separation is carried out in situ, and the NGH phase changes are small. Therefore, assuming that there is no phase transition, all NGH is solid and the particle size of NGH is the same as that of sand. NGH reservoir parameters are mainly sediment particle size, porosity, and saturation. During the separation process, the above parameters are reflected in the particle size, inlet NGH phase, and sand phase volume fraction in the mixed slurry. According to the analysis results of the particle size distribution of marine gas hydrate sediments in the South China Sea mentioned above, the particle size of the sediments is mainly less than 100 μm, and most of them are about 30 μm. Therefore, in this paper, when the volume fraction of NGH and sand is 10 and 15%, respectively, the particle diameter is 30 μm, and the inlet velocity is calculated from a flow rate of 15 m^3/h. The physical parameters used in this paper are shown in Table 2.

Table 2. Physical Parameters of Media

media	density (kg/m^3)	viscosity (kg/m/s)
seawater	1025	0.0017
sand	2600	
NGH	910	

Due to the short working time from the initial to the stable operation of the NGH hydrocyclone in actual working conditions, in addition, existing scholars use steady-state simulations and apply their results to a real device.[32,33] Therefore, in this paper, ANSYS Fluent18.0 software was used for numerical simulations. Furthermore, the simulation was carried out in a three-dimensional (3D) model, with a steady-state, double precision implicit solver adopted. The SIMPLE algorithm scheme, which uses a combination of continuity and momentum equations to derive an equation for pressure, was used. The QUICK spatial discretization scheme was applied, as it is reported to be useful for swirling flows. The inlet condition was the velocity inlet. The outlet was the pressure outlet, and the no-slip boundary condition was used for the wall boundary.

2.2.3. Calculation Method of Separation Efficiency and Pressure Drop. The separation efficiency is an important index of the separation performance of the spiral separator. The sand discharge amount and NGH recovery amount are considered at the outlet section in this device. Separation efficiency is generally defined as the ratio of outlet phase mass to inlet phase mass.

$$E_1 = \frac{M_{o1}}{M_{i1}} \times 100\%$$

$$E_2 = \frac{M_{o2}}{M_{i2}} \times 100\% \quad (7)$$

where E_1 is the natural gas hydrate recovery efficiency %, M_{o1} is the natural gas hydrate mass flow rate at the vortex finder (natural gas hydrate recovery) outlet kg/s, M_{i1} is the natural gas hydrate mass flow rate at the inlet kg/s, E_2 is the desanding efficiency %, M_{o2} is the sand mass flow rate at the spigot (desanding) outlet kg/s, and M_{i2} is the sand mass flow rate at the inlet, kg/s.

As we know, the low-pressure drop of the separator represents its low energy consumption. Thus, the pressure drop is also one of the most important indexes to evaluate the performance of the separator.

The pressure drop is shown in the below equation

$$\triangle p_1 = p_0 - p_1$$

$$\triangle p_2 = p_0 - p_2 \quad (8)$$

where Δp_1 is the natural gas hydrate pressure drop Pa, p_0 is the inlet pressure Pa, p_1 is the pressure at the vortex finder (NGH recovery) outlet Pa, Δp_2 is the sand pressure drop Pa, and p_2 is the pressure at the spigot (desanding) outlet Pa.

2.2.4. Influence of Structural Parameters on the Sensitivity Analysis Method. The degree of the influence of structural parameters has an important guide for the design and performance optimization of the NGH hydrocyclone. Therefore, a sensitivity analysis was carried out. Sensitivity analysis is a research method for the stability of the analysis system affected by the associated parameters in the parameter optimization analysis method. Its definition assumes that there are N_i influencing factors in a system, and the system characteristics are $F = f(x_1, x_2, \cdots x_{N_i})$. The system characteristic in this reference state is $F^* = f(X^*)$. Parameter sensitivity analysis is defined as the tendency and degree of the variation system characteristic F of the obtained parameter to deviate from the reference state F^* when the associated parameter varies within the possible variation range.

https://doi.org/10.1021/acsomega.3c02920
ACS Omega 2023, 8, 28531−28542

In the study, E_1 and E_2 were taken as the system characteristics, the structural parameter changes of the NGH hydrocyclone were taken as the relevant parameters, and the reference state was defined as the E_1 and E_2 of the NGH hydrocyclone with the initial structure. The degree of deviation S_i is the degree to which E_1 and E_2 deviate from the initial efficiency when the structural parameters change; its calculation formula is shown in 9

$$S_i = \frac{F - F^*}{F} \times 100\% \tag{9}$$

The maximum deviation degree $S_{imax} - S_{imin}$ of the system is a characteristic of the same associated parameter from the reference state. It shows that the structural parameter has a greater influence on the performance, and this parameter change is more sensitive. The main parameters were taken as associated parameters, as shown in Table 3.

Table 3. Main Related Parameters Affecting the Separation Efficiency of the NGH Hydrocyclone

numbers	structure	associated parameters
S_1	spiral inlet	steady flow cone angle
S_2		B
S_3		N
S_4		number of inlet spiral heads
S_5	vortex finder	d_0
S_6		insertion depth of the vortex finder
S_7	conic section	β
S_8	cylindrical section	H
S_9	spigot	d_s

2.3. Structure and Meshing of the Axial-Flow Inlet Hydrocyclone. The separation principle is shown in Figure 2b. It is the diversion of the mixed slurry through the inlet annulus and the spiral guide vanes (converting the axial transport velocity of the slurry into a tangential velocity) and preseparation; under the action of centrifugal force, the NGH phase with lower density has a directional flow. The sand phase with higher density tends to be close to the wall so as to achieve the effect of preseparation and then enters the combined vortex-like centrifugal field inside the separator for fine separation again. NGH enters the inner vortex and is recovered from the NGH recovery outlet. The sand enters the outer vortex and is discharged from the desanding outlet. Finally, the solid−solid−liquid three-phase separation is completed.

The axial-flow inlet hydrocyclone is mainly composed of a spiral inlet and preseparation section, a cylindrical section, a conical section, a vortex finder outlet, and a spigot outlet. The geometry diagram, meshed structure, and initial dimensions are shown in Figure 4 and Table 4, respectively. The

Table 4. Dimensions of the Axial-Flow Inlet Hydrocyclone

D (mm)	B (mm)	N	d_0/D	d_s/D	β (°)	m	α (°)	H (mm)
100	24	2	0.32	0.26	10	2	10	65

computational domain of the axial-flow NGH hydrocyclone was meshed. The computational domain consists of a mixture of structured and unstructured grids, as shown in Figure 4b.

2.4. Grid Independence and Model Validation. To ensure the independence of the grid number in the numerical simulation, the model with initial structural parameters was taken as an example; the NGH recovery efficiency and desanding efficiency were compared under grid numbers 50, 100, 150, 200, and 250k. As shown in Figure 5, as the number of grids increases, the tangential velocity and static pressure stabilize and change very little after 150k. Therefore, considering the computational accuracy and time consumption, the computational domain of the axial-flow inlet hydrocyclone is divided into 150k cells.

To verify the model, single sand phase separation was investigated by numerical simulation and experimental tests. As shown in Figure 6, the desanding efficiency and pressure drop were compared. The results obtained by the numerical simulation are higher than those measured by the experiment, but there is a small error. And the desanding efficiency and pressure drop increase continuously with the increase of inlet velocity. The error of desanding efficiency obtained from the numerical simulation and experiment is shown in Table 5. The minimum, maximum, and average errors between the simulated and experimental values of desanding efficiency are 4.86, 8.27, and 6.20%, respectively. The numerical simulation results are generally consistent with the experimental results. The main reason is that the numerical simulation simplifies the actual process to a certain extent. The median particle size used in the numerical simulation is 30 μm, and the density of water and sand is slightly different.

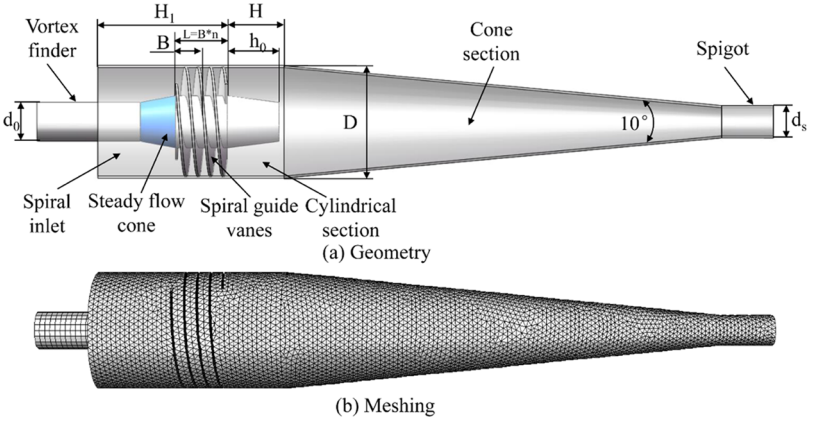

Figure 4. (a) Simplified structure of the NGH hydrocyclone and (b) the meshed structure of the NGH hydrocyclone.

https://doi.org/10.1021/acsomega.3c02920
ACS Omega 2023, 8, 28531−28542

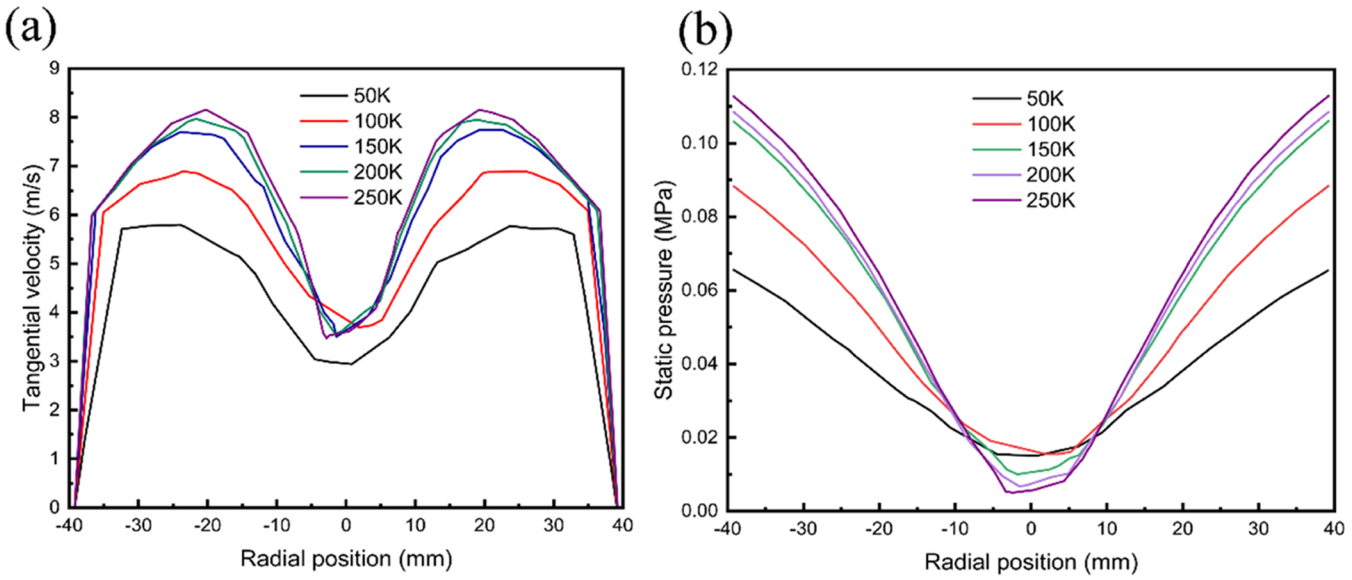

Figure 5. Grid-independency check: (a) tangential velocity and (b) static pressure.

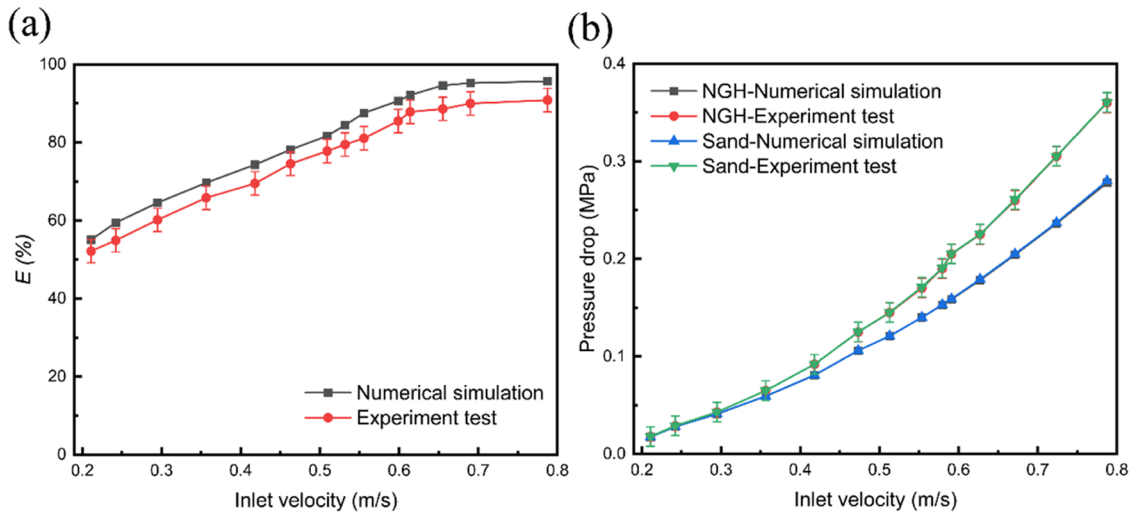

Figure 6. (a) Comparison of the desanding efficiency between experimental tests and numerical simulations and (b) the comparison of the pressure drop between experimental tests and numerical simulations.

Table 5. Efficiency and Error of the Single Desanding Phase at Different Inlet Velocities

inlet velocity (m/s)	desanding efficiency—simulation (%)	desanding efficiency—experiment (%)	relative error (%)
0.211	55.10	52.14	5.68
0.242	59.46	54.92	8.27
0.295	64.54	60.15	7.29
0.356	69.66	65.82	5.83
0.418	74.32	69.51	6.92
0.463	78.15	74.53	4.86
0.509	81.66	77.80	4.96
0.532	84.42	79.47	6.23
0.556	87.54	81.08	7.97
0.599	90.62	85.49	6.00
0.614	92.12	87.84	4.87
0.655	94.61	88.59	6.79
0.790	95.23	89.97	5.84
0.756	95.68	90.83	5.34

3. RESULTS AND DISCUSSION

3.1. Effect Sensitivity. From the comparison of the degree of deviation of E for the associated parameters in Figure 7, it can be seen that the influence of each structural parameter on the performance is different. E caused by the change level of the selected parameters is reduced or increased, which shows that the selection of the change level of the associated parameters is reasonable. Considering the influence of structural parameters on E_1 and E_2, it can be concluded that the most influential factors are the spiral pitch, vortex finder diameter, and spigot diameter. The number of turns and heads of the spiral deflector, the insertion depth of the vortex finder, and the cone angle take the second place. The influence of the cone angle of the inlet steady flow cone and the length of the cylindrical section is the least.

It can be seen from Figure 8 that the order of the maximum deviation degree from strong to weak in the evaluation of E_1 from each associated parameter is $S_5 > S_9 > S_2 > S_3 > S_7 > S_4 > S_1 > S_6 > S_8$. From E_2, the order of the maximum deviation

https://doi.org/10.1021/acsomega.3c02920
ACS Omega 2023, 8, 28531−28542

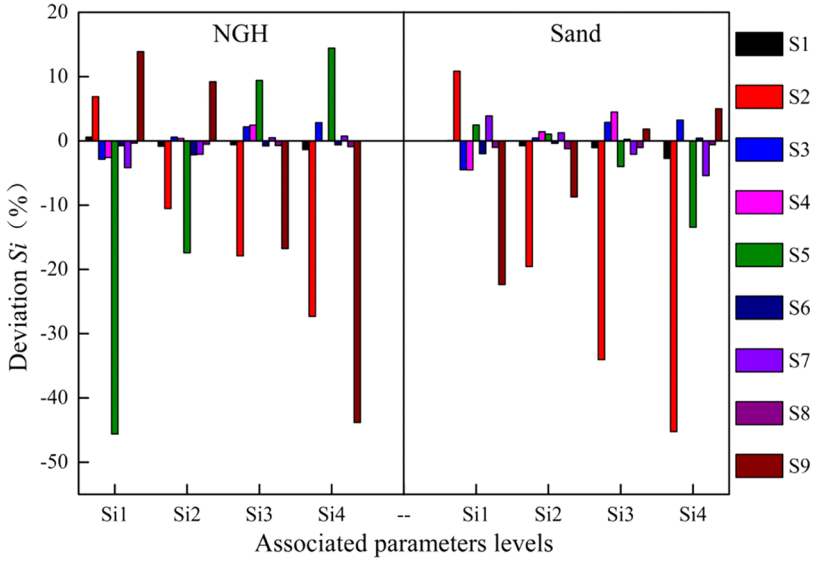

Figure 7. Comparison of the deviation of separation efficiency within the associated parameters levels.

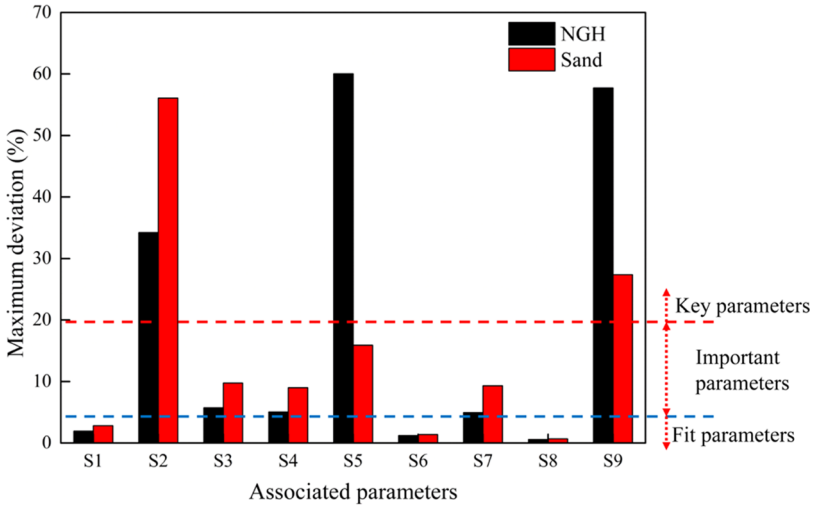

Figure 8. Comparison of the maximum deviation of separation efficiency within the associated parameters.

degree from strong to weak is $S_2 > S_9 > S_5 > S_3 > S_7 > S_4 > S_1 > S_6 > S_8$. Considering E_1 and E_2 comprehensively, the structural parameters can be divided into three categories: Specifically, key parameters for which the maximum deviation value is basically more than 20% are the parameters with the greatest influence, including S_2, S_5, and S_9. More important parameters for which the maximum deviation value is 5−20% are parameters with a large degree of influence, including S_7 and S_3. Fit parameters for which the maximum deviation value is less than 5% are the parameters with the least influence, including S_1, S_4, S_6, and S_8. The key parameters and important parameters should be considered in design optimization when designing the structure. The fit parameters can be appropriately ignored.

3.2. Effect Law. From the above sensitivity analysis results of the influence of structural parameters, it can be seen that the key and important parameters have a great impact on the separation performance, while the influence of fit parameters on the separation performance is very small. Therefore, key and important parameters are selected when carrying out specific impact law analysis. However, the specific impact of the structural parameters of the spiral inlet on separation performance has been revealed in previously published papers.[14] In this paper, the specific parameters selected do not duplicate the spiral inlet parameters. The specific parameters selected are the vortex finder diameter, the spigot diameter, and the cone angle.

3.2.1. Effect of d_0/D. d_0/D affects the distribution of the fluid in the separator between the underflow and the overflow, so it also determines the performance of the NGH hydrocyclone to a certain extent. Five configurations of d_0/D 0.24, 0.28, 0.32, 0.36, and 0.40 were studied, and their structural schematic diagrams are shown in Figure 9a.

Figure 9 shows the effect of d_0/D on the separation performance of the axial-flow NGH hydrocyclone. It can be seen from Figure 9e that the change of d_0/D has an obvious effect on E. With the increase of d_0/D, the NGH recovery efficiency increases sharply, and the desanding efficiency decreases continuously. Within the research range, the NGH recovery efficiency increases by about 40%, and the desanding efficiency decreases by about 15%. As shown in Figure 9f, as d_0/D increases, the pressure drop increases, but the increased

https://doi.org/10.1021/acsomega.3c02920
ACS Omega 2023, 8, 28531−28542

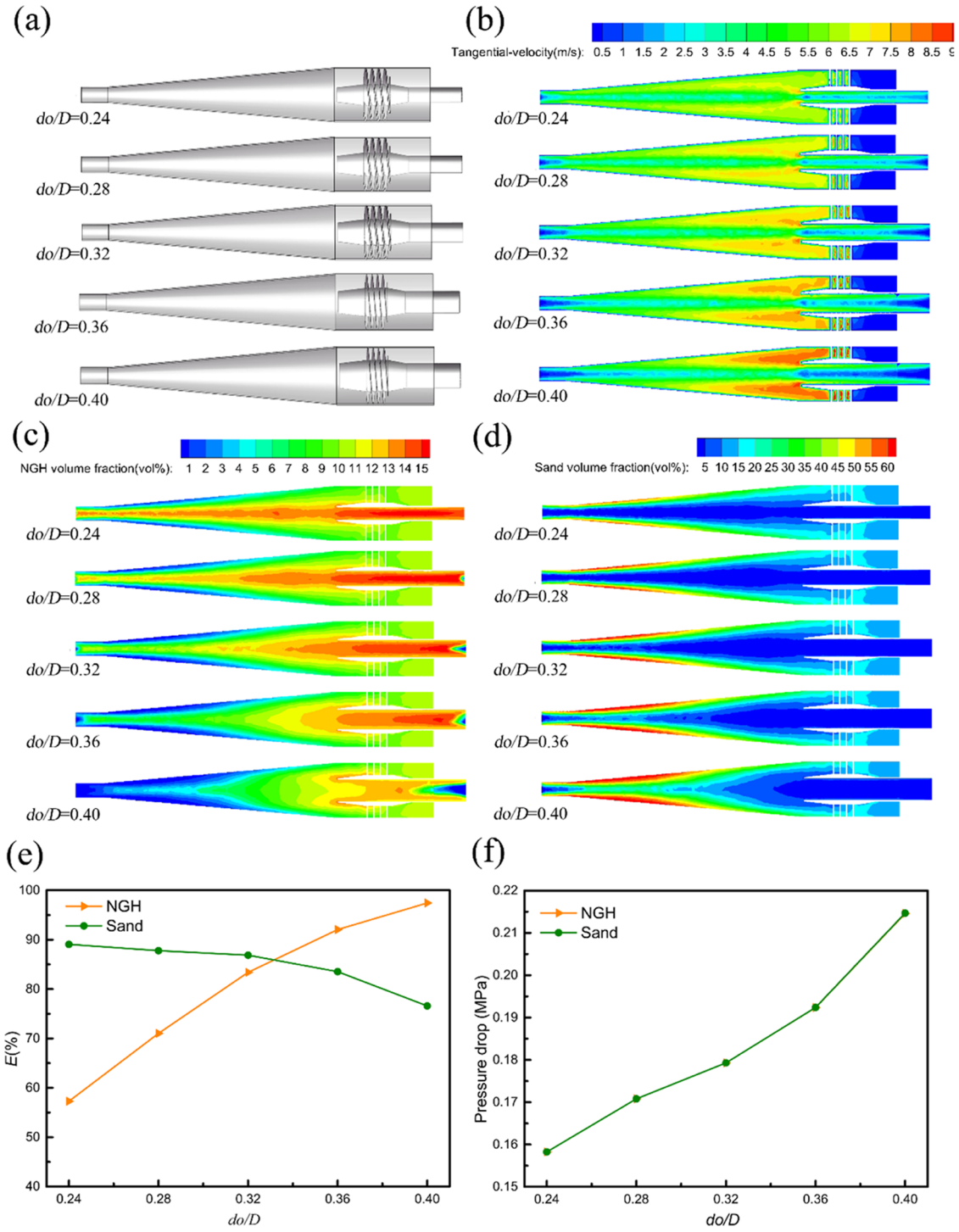

Figure 9. Effect of d_0/D on separation performance: (a) structural diagram; (b) tangential velocity; (c) NGH volume fraction; (d) sand volume fraction; (e) NGH recovery efficiency and desanding efficiency; and (f) pressure drop.

range is small. In the research range, the increased amplitude is about 0.07 MPa. d_0/D has less effect on the pressure drop. Figure 9c,d is the cloud diagrams of the volume fraction distribution of sand and NGH phases. As d_0/D increases, the volume fraction of the sand phase near the wall and the sand outlet decreases. However, the volume fraction of the NGH phase increases near the center. The main reason is explained in Figure 9b; it can be seen that with the increase of d_0/D, the distribution law of the tangential velocity remains unchanged, but the value increases sharply, which increases the centrifugal force on the discrete-phase particles. Further from Figure 9a, it can be seen that the larger the d_0/D, the smaller the annular space of the inlet. When the Q is determined, the inlet velocity is larger and the NGH outlet flow rate is larger. Therefore, it is necessary to choose an appropriate d_0/D to balance NGH recovery efficiency and sand removal efficiency.

3.2.2. Effect of d_s/D. There are five different axial-flow NGH hydrocyclone with a d_s/D of 0.18, 0.22, 0.26, 0.30, and 0.34, respectively. The structural schematic diagram is shown in

https://doi.org/10.1021/acsomega.3c02920
ACS Omega 2023, 8, 28531−28542

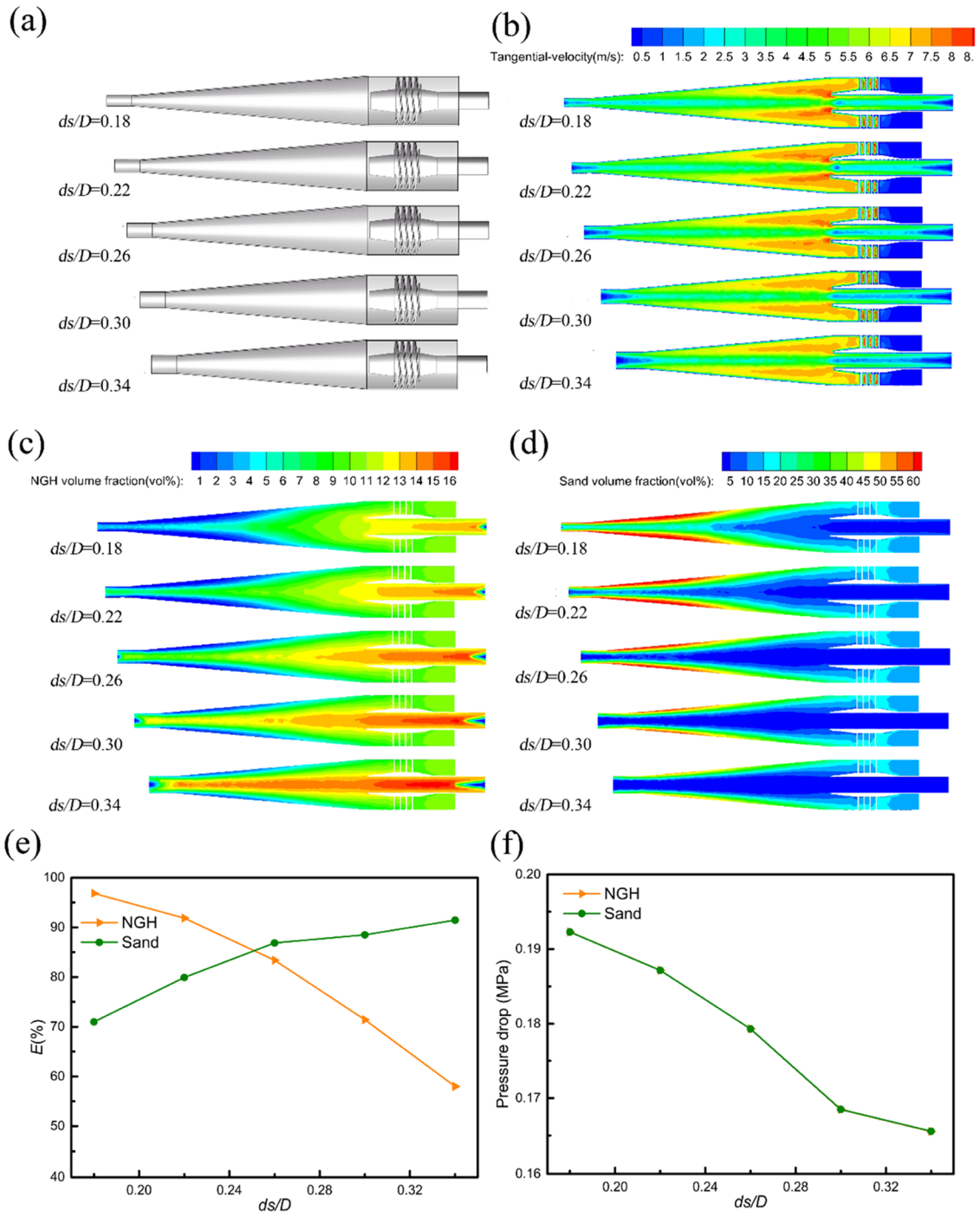

Figure 10. Effect of d_s/D on separation performance: (a) structural diagram; (b) tangential velocity; (c) NGH volume fraction; (d) sand volume fraction; (e) NGH recovery efficiency and desanding efficiency; and (f) pressure drop.

Figure 10a. It can be seen that the larger the d_s/D, the shorter the cone section and the shorter the overall length.

Figure 10 shows the effect of d_s/D on the separation performance. Figure 10e shows the change of E and pressure drop. It can be seen that the change of d_s/D has a significant impact on E. With the increase of d_s/D, the NGH recovery efficiency decreases sharply, and the desanding efficiency continues to increase. Within the research range, the NGH recovery efficiency decreases by about 40% and the desanding efficiency increases by about 20%. As shown in Figure 10f, with the increase of d_s/D, the pressure drop decreased, but the magnitude of the decrease was not large, and the pressure drop value of both outlets was almost equal. In the study range, it decreased by about 0.03 MPa. Figure 10c,d shows the cloud diagrams of the volume fraction distribution of sand and NGH phases, and it can be seen that with the increase of d_s/D, the volume fraction of the sand phase near the wall increases. The NGH phase volume fraction increases in the center. The main reason can be found in Figure 10a,b; with the increase of d_s/D, the distribution law of the tangential velocity remains unchanged, and its value decreases sharply, indicating that the increase of d_s/D will decrease the centrifugal force on the discrete-phase particles, and increase the flow out of the sand

https://doi.org/10.1021/acsomega.3c02920
ACS Omega 2023, 8, 28531−28542

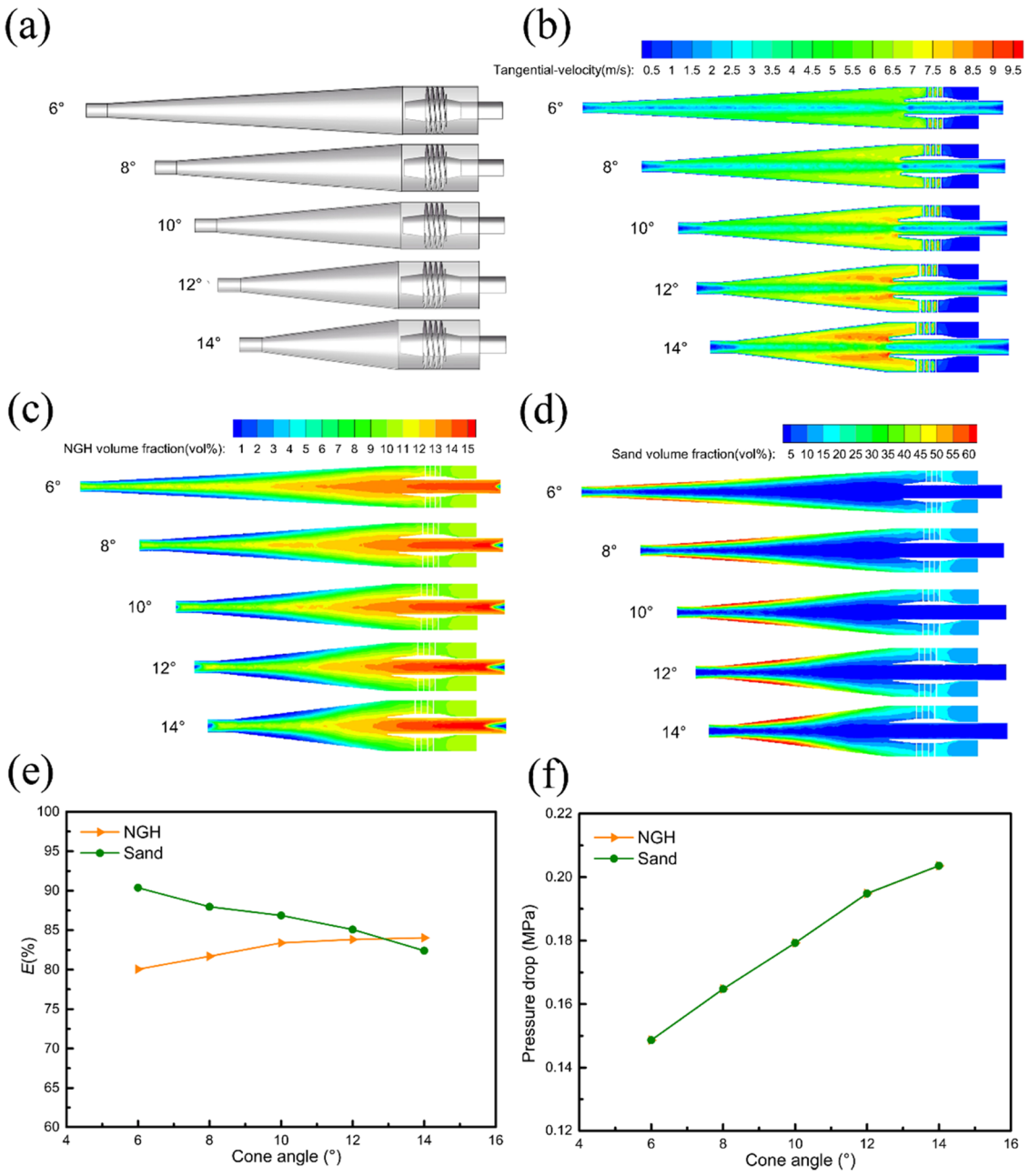

Figure 11. Effect of the cone angle on separation performance: (a) structural diagram; (b) tangential velocity; (c) NGH volume fraction; (d) sand volume fraction; (e) NGH recovery efficiency and desanding efficiency; and (f) pressure drop.

outlet, which will cause more sand phase to be discharged from it.

It can be seen from the above analysis that d_s/D has a great influence on the NGH recovery efficiency and desanding efficiency of the axial-flow NGH hydrocyclone, has a relatively great influence on the tangential velocity and phase distribution, and has a relatively large influence on the pressure drop. Therefore, it is necessary to choose an appropriate d_s/D to balance separation performance indicators such as separation efficiency and pressure drop.

3.2.3. Effect of β. The influence of β on the separation performance of the axial-flow inlet NGH hydrocyclone is shown in Figure 11. β is 6, 8, 10, 12, and 14°, respectively.

Figure 11e,f shows the E and pressure drop change curves of axial-flow inlet NGH hydrocyclones with different β. It can be seen from the figure that with the increase of β, the NGH recovery efficiency increases, but the desanding efficiency decreases. On the whole, the NGH recovery efficiency and desanding efficiency change greatly. The desanding efficiency decreases by about 8% and the NGH recovery efficiency increases by about 4%. It can be seen from Figure 11f that with the increase β, the pressure drop continuously increases, and the pressure drop value at both outlets is relatively close; In the study range, the increased amplitude of pressure drop is about 0.06 MPa. It shows that the change in β has a great influence on the energy consumption of the axial-flow inlet NGH hydrocyclone. Figure 11c,d is a cloud diagram of the volume fraction distribution of the sand phase and NGH phase with different β. It can be seen from the figure that with the increase in β, the volume fraction of the sand phase near the wall

https://doi.org/10.1021/acsomega.3c02920
ACS Omega 2023, 8, 28531−28542

decreases, while the volume fraction of the NGH phase near the center increases. The structural schematic diagram is shown in Figure 11a. It can be seen that the larger the β, the shorter the cone section of the axial-flow inlet NGH hydrocyclone. The cone section is one of the main separation areas. β determines the length of the cone section, tangential velocity, and residence time of the particles. It can be seen from Figure 11b that with the increase in β, the distribution law of the tangential velocity will not change, and its value will increase sharply. Meanwhile, the flow at the NGH recovery outlet and the centrifugal force will be increased, and the residence time of discrete-phase particles will be shortened. The change in β has a great influence on the separation efficiency.

From the above analysis results, it can be seen that the change in β has a great impact on the separation performance in the axial-flow inlet NGH hydrocyclone. Therefore, it is necessary to select a suitable β to balance the separation performance.

4. CONCLUSIONS

In this paper, the effect of structural parameters on separation performance was also developed to guide the design of NGH separators by experiments and numerical simulations. The main conclusions obtained are as follows:

(1) Taking NGH recovery efficiency and desanding efficiency as comprehensive evaluation indicators, the most influential factors are the spiral pitch, the vortex finder diameter, and the spigot diameter. The second most influential factors are the spiral turn number and the cone angle of the cone section. Other parameters have the least influence. It is suggested that the spiral pitch of the spiral inlet section, the vortex finder diameter, and the spigot diameter should be put in the first place, the cone angle and the spiral turn number should be put in the second place, and other parameters should be put in the last place when designing the axial-flow inlet NGH hydrocyclone.

(2) The NGH recovery efficiency increases when d_s/D decreases and d_0/D and the cone angle increase. The desanding efficiency increases when d_0/D and the cone angle decreases and d_s/D increases. The pressure drop decreases when d_0/D and the cone angle decrease and d_s/D increases. It is recommended to match the appropriate vortex finder diameter, spigot diameter, and cone angle to improve the separation efficiency.

AUTHOR INFORMATION

Corresponding Author

Shunzuo Qiu − *Department of International Applied Technology, Yibin University, Yibin 644000, China;* orcid.org/0000-0001-9218-633X; Phone: 18782944071; Email: qiushunzuo@163.com

Authors

Lin Zhong − *Department of Mechatronic Engineering, Southwest Petroleum University, Chengdu 610500, China*

Guorong Wang − *Department of Mechatronic Engineering, Southwest Petroleum University, Chengdu 610500, China*

Xing Fang − *Department of Mechatronic Engineering, Southwest Petroleum University, Chengdu 610500, China*

Yan Yang − *Department of International Applied Technology, Yibin University, Yibin 644000, China*

Qin Liu − *Department of International Applied Technology, Yibin University, Yibin 644000, China*

Complete contact information is available at: https://pubs.acs.org/10.1021/acsomega.3c02920

Author Contributions

G.W.: Conceptualization, supervision, and funding acquisition; S.Q.: investigation, writing—original draft, and funding acquisition; L.Z.: methodology and validation; X.F.: software; Y.Y.: writing—revision and validation; and Q.L.: writing—revision and validation.

Notes

The authors declare no competing financial interest.

ACKNOWLEDGMENTS

The authors are grateful to the Science and Technology Innovation in Sichuan Province (Seedling Project) [2022074], the "Sailing" project of Yibin University [2021QH020, 2022QH19], and the National Key R&D Program of China [2019YFC0312305].

NOMENCLATURE

NGH, natural gas hydrate; B, spiral pitch (mm); N, number of spiral turns; d_0, diameters of the vortex finder (mm); d_s, diameter of the spigot (mm); α, cone angle of the steady flow cone (°); D, dominant diameter (mm); β, cone angle of the cone section (°); Q, inlet flow rate (m^3/h); H, length of the cylindrical section (mm); H_1, length of the spiral inlet (mm); V, suspension volume (L); C, inlet solid content (g/L); C_2, sand slurry solid content (g/L); E, separation efficiency (%); E_1, NGH recovery efficiency (%); E_2, desanding efficiency (%); Q_2, sand slurry flow rate (m^3/h)

REFERENCES

(1) Chong, Z. R.; Yang, S. H. B.; Babu, P.; Linga, P.; Li, X. Review of natural gas hydrates as an energy resource: Prospects and challenges. *Appl. Energy* **2016**, *162*, 1633−1652.

(2) Kvenvolden, K. A. Potential effects of gas hydrate on human welfare. *Proc. Natl. Acad. Sci. U.S.A.* **1999**, *96*, 3420−3426.

(3) Makogon, Y. F. Natural gas hydrates - A promising source of energy. *J. Nat. Gas Sci. Eng.* **2010**, *2*, 49−59.

(4) Li, J.-f.; Ye, J.-l.; Qin, X.-w.; Qiu, H.-j.; Wu, N.-y.; Lu, H.-l.; Xie, W.; Lu, J.; Peng, F.; Xu, Z.; Lu, C.; Kuang, Z.; Wei, J.; Liang, Q.; Lu, H.; Kou, B. The first offshore natural gas hydrate production test in South China Sea. *China Geol.* **2018**, *1*, 5−16.

(5) Zhou, S. W.; Chen, W.; Li, Q. P.; Zhou, J. L.; Shi, H. S. Research on the solid fluidization well testing and production for shallow non-diagenetic natural gas hydrate in deep water area. *China Offshore Oil Gas* **2017**, *29*, 1−8.

(6) Lu, J. S.; Wu, S. T.; Li, D. L.; Liang, D. Q.; Wei, W.; He, Y.; Shi, L. L.; Deng, F. C.; Xiong, Y. M. Solid Phase Control Strategy during the Exploitation of Marine Gas Hydrates. *Adv. New Renewable Energy* **2022**, *10*, 137−145.

(7) Hou, L.; Yang, J. H.; Liu, Z. X.; Jiao, J. Current status and suggestions on development of marine gas hydrate technologies in China. *Word Pet. Ind.* **2021**, *28*, 17−22.

(8) Yan, C.; Ren, X.; Cheng, Y.; Song, B.; Li, Y.; Tian, W. Geomechanical issues in the exploitation of natural gas hydrate. *Gondwana Res.* **2020**, *81*, 403−422.

(9) Wu, P.; Li, Y.; Wang, L.; Sun, X.; Wu, D.; He, Y.; Li, Q.; Song, Y. Hydrate-bearing sediment of the South China Sea: Microstructure and mechanical characteristics. *Eng. Geol.* **2022**, *307*, No. 106782.

(10) Wu, P.; Li, Y.; Sun, X.; Liu, W.; Song, Y. Mechanical Characteristics of Hydrate-Bearing Sediment: A Review. *Energy Fuels* **2021**, *35*, 1041−1057.
(11) Ding, J.; Cheng, Y.; Yan, C.; Song, B.; Sun, H.; Teng, F. Experimental study of sand control in a natural gas hydrate reservoir in the South China sea. *Int. J. Hydrogen Energy* **2019**, *44*, 23639−23648.
(12) Zhang, Y.; Wang, W.; Zhang, P.; Li, G.; Tian, S.; Lu, J.; Zhang, B. A Solution to Sand Production from Natural Gas Hydrate Deposits with Radial Wells: Combined Gravel Packing and Sand Screen. *J. Mar. Sci. Eng.* **2022**, *10*, No. 71.
(13) Li, Y.; Wu, N.; Ning, F.; Gao, D.; Hao, X.; Chen, Q.; Liu, C.; Sun, J. Hydrate-induced clogging of sand-control screen and its implication on hydrate production operation. *Energy* **2020**, *206*, No. 118030.
(14) Qiu, S. Z.; Wang, T.; Wang, G. R.; Zhong, L.; Fang, X. Effect of Spiral Inlet Geometric Parameters on the Performance of Hydrocyclones Used for In Situ Desanding and Natural Gas Hydrate Recovery in the Subsea. *ACS Omega* **2023**, *8*, 5426−5436.
(15) Zeng, X.; Zhao, L.; Zhao, W.; Hou, M.; Zhu, F.; Fan, G.; Yan, C. Experimental Study on a Novel Axial Separator for Oil-Water Separation. *Ind. Eng. Chem. Res.* **2020**, *59*, 21177−21186.
(16) Patel, M.; Patel, J.; Pawar, Y.; Patel, N.; Shah, M. Membrane-based downhole oil-water separation (DOWS) technology: an alternative to hydrocyclone-based DOWS. *J. Pet. Explor. Prod. Technol.* **2020**, *10*, 2079−2088.
(17) Mo, S. P.; Chen, X. Q.; Chen, Y.; Yang, Z. Effect of geometric parameters of liquid-gas separator units on phase separation performance. *Korean J. Chem. Eng.* **2015**, *32*, 1243−1248.
(18) Xu, B.; Zhang, X.; Zhao, L.; Jiang, M.; Liu, L.; Xia, H. Structure design and preliminary experimental investigation on oil-water separation performance of a novel helix separator. *Sep. Sci. Technol.* **2021**, *56*, 2680−2691.
(19) Zhao, Z.; Zhou, L.; Liu, B.; Cao, W. Computational fluid dynamics and experimental investigation of inlet flow rate effects on separation performance of desanding hydrocyclone. *Powder Technol.* **2022**, *402*, No. 117363.
(20) Sun, Y. Q.; Yu, J. Z.; Wang, W. B.; Yang, S. L.; Hu, X.; Feng, J. G. Design of vortex finder structure for decreasing the pressure drop of a cyclone separator. *Korean J. Chem. Eng.* **2020**, *37*, 743−754.
(21) Tian, J.; Ni, L.; Song, T.; Zhao, J. CFD simulation of hydrocyclone-separation performance influenced by reflux device and different vortex-finder lengths. *Sep. Purif. Technol.* **2020**, *233*, No. 116013.
(22) Chang, Y.-l.; Ti, W.-q.; Wang, H.-l.; Zhou, S.-w.; Huang, Y.; Li, J.; Wang, G.; Fu, Q.; Lin, H.; Wu, J. Hydrocyclone used for in-situ sand removal of natural gas-hydrate in the subsea. *Fuel* **2021**, *285*, No. 119075.
(23) Nie, Q.; Zhang, S.; Huang, Y.; Yi, X.; Wu, J. Numerical and Experimental Investigation on Safety of Downhole Solid-Liquid Separator for Natural Gas Hydrate Exploitation. *Energies* **2022**, *15*, No. 5649.
(24) Dong, H.; Wu, K. S.; Kuang, Y. C.; Dai, M. L. Study on separation law of hydrate slurry in hydrocyclone based on CFD-DEM. *J. Zhejiang Univ. (Eng. Sci.)* **2018**, *52*, 1811−1820.
(25) Dai, M. L. *Study on Multiphase Flow and Separation of Hydrate Slurry in Spiral Tube*; Southwest Petroleum University, 2017.
(26) Qiu, S.; Wang, G.; Zhou, S.; Liu, Q.; Zhong, L.; Wang, L. The downhole hydrocyclone separator for purifying natural gas hydrate:structure design, optimization, and performance. *Sep. Sci. Technol.* **2020**, *55*, 564−574.
(27) Fang, X.; Wang, G.; Zhong, L.; Qiu, S.; Wang, D. A CFD−DEM analysis of the de-cementation behavior of weakly cemented gas hydrate−bearing sediments in a hydrocyclone separator. *Part. Sci. Technol.* **2022**, 812−823.
(28) Qiu, S.; Wang, G.; Wang, L.; Fang, X. A Downhole Hydrocyclone for the Recovery of Natural Gas Hydrates and Desanding: The CFD Simulation of the Flow Field and Separation Performance. *Energies* **2019**, *12*, No. 3257.
(29) Chen, H.; Lv, B.; Fu, L. Q.; Wu, W. K. Separation and purification of natural gas hydrate slurry mixture by hydrocyclone. *Mod. Chem. Ind.* **2017**, *37*, 155−159.
(30) Qiu, S.; Wang, G. Effects of Reservoir Parameters on Separation Behaviors of the Spiral Separator for Purifying Natural Gas Hydrate. *Energies* **2020**, *13*, No. 5346.
(31) Zhang, C.; Cui, B.; Wei, D.; Lu, S. Effects of underflow orifice diameter on the hydrocyclone separation performance with different feed size distributions. *Powder Technol.* **2019**, *355*, 481−494.
(32) Vieira, L. G. M.; Barrozo, M. A. S. Effect of vortex finder diameter on the performance of a novel hydrocyclone separator. *Miner. Eng.* **2014**, *57*, 50−56.
(33) Zhen-bo, W.; Yi, M.; You-hai, J. Simulation and experiment of flow field in axial-flow hydrocyclone. *Chem. Eng. Res. Des.* **2011**, *89*, 603−610.

https://doi.org/10.1021/acsomega.3c02920
ACS Omega 2023, 8, 28531−28542